



A novel visible-light-driven photocatalyst Ag₂O/AgI with highly enhanced photocatalytic performances



Duo Heng Cui ^a, Yi Fan Zheng ^b, Xu Chun Song ^{a,*}

^a Department of Chemistry, Fujian Normal University, Fuzhou 350007, PR China

^b Research Center of Analysis and Measurement, Zhejiang University of Technology, Hangzhou 310014, PR China

ARTICLE INFO

Article history:

Received 17 October 2016

Received in revised form

12 December 2016

Accepted 12 January 2017

Available online 16 January 2017

Keywords:

Ag₂O/AgI

Ag NPs

Photocatalytic

ABSTRACT

A series of heterojunction Ag₂O/AgI photocatalysts with different Ag₂O contents were successfully prepared through a facile two-step precipitation process at room temperature. The as-synthesized samples were measured in detail by XRD, EDS, XPS, SEM and DRS. The results showed that spherical Ag₂O nanoparticles with diameter about 100–300 nm were uniformly distributed on the surface of AgI leading to the formation of Ag₂O/AgI heterojunction. The photocatalytic activities of the obtained photocatalysts were evaluated by photocatalytic degradation of Rhodamine B (RhB) under visible light irradiation. The Ag₂O/AgI with molar ratio of 1:1 showed the highest photocatalytic activities compared to the pure Ag₂O and AgI with almost all RhB decomposed in 25 min. During photocatalytic process the visible light induced photogenerated electrons can be captured by Ag⁺ ions on the surface lattice of heterojunction to form plasmonic Ag nanoparticles, which may promote the interfacial charge transfer. The enhanced photocatalytic activity was then largely attributed to the synergistic effects of heterojunction Ag₂O/AgI/Ag and the efficient separation of photogenerated electron–hole pairs. This research may provide a novel Ag₂O/AgI heterojunction with assistant of plasmonic Ag NPs to generate efficient, stable, and recyclable visible-light-driven plasmonic photocatalysts. The photocatalytic reaction kinetics and possible photocatalytic mechanism for this highly efficient photocatalysts were also proposed.

© 2017 Elsevier B.V. All rights reserved.

1. Introduction

In recent decades, semiconductor-based photocatalysts have attracted considerable attention for their availability of solar energy conversion and potential application on solving the aquatic environmental issues. Among them, titanium dioxide (TiO₂) with high physical and chemical stability, low price, nontoxicity, effectivity has been regarded as one of the most promising semiconductor catalysts and extensively used in the degradation of organic pollutants [1,2]. However, relatively wide band gap of TiO₂ limits its photo-response only to ultraviolet range, which occupies only a small portion of solar light (less than 5%) [3]. Moreover, there is a deficiency in rapid recombination of photogenerated electron–hole pairs before they transfer to the photocatalyst surface, which leads to low quantum efficiency [4]. Therefore, it is indispensable to exploit novel visible light induced photocatalysts with high activities [5,6]. Recently, Ag-based semiconductors, which exhibit high

initial photocatalytic activity [7,8], have aroused more and more attention.

Among the Ag-based semiconductors, Ag₂O with favorable narrow band gap (1.2 eV) is suitable for applications in photocatalysis in the visible light region. It has been found to have high photocatalytic activity under visible light irradiation with also much high stability [9–13]. Ag₂O nanoparticles as visible light active components have also been used to combine with other semiconductors or metal and nonmetal to form composited photocatalysts, such as ZnO/Ag₂O [14], Ag₂O/TiO₂ [9,15], Ag₂O/g-C₃N₄ [16], Ag₂O/AgBr [17], Ag₂O/Bi₂WO₆ [18] and Ag/AgI/BiOI [6], which all displayed excellent photocatalytic performance under visible light irradiation.

Recently, AgI with a small band gap (2.80 eV) have been coupled with TiO₂ as a highly efficient visible light sensitive material, which also showed enhanced visible light induce performance [19]. However, silver halides (AgX, X = Cl, Br, I), as photosensitive semiconductor materials, is instable in pure crystal form, which have been commonly applied in photographic films [20]. If the AgX materials are coated on certain semiconductor materials, it could

* Corresponding author.

E-mail address: songxuchunfj@163.com (X.C. Song).

improve the stability and the photocatalytic activity of the hybrid materials, such as $\text{AgX}/\text{Ag}_3\text{PO}_4$ [21,22], AgI/TiO_2 [1,2,23,24], AgX/BiPO_4 [25–27], $\text{AgX}/\text{Ag}_2\text{CO}_3$ ($\text{X} = \text{Cl}, \text{I}$) [28], $\text{AgI}/\text{Bi}_2\text{O}_2\text{CO}_3$ [29] and so on. Thus, we have attempted to combine Ag_2O with AgI to construct $\text{Ag}_2\text{O}/\text{AgI}$ composites, and to the best of our knowledge there is no report on this kind novel $\text{Ag}_2\text{O}/\text{AgI}$ heterojunction.

In this work, $\text{Ag}_2\text{O}/\text{AgI}$ photocatalysts were successfully synthesized through a facile two-step precipitation process at room temperature. The as-prepared products were characterized by XRD, SEM, XPS, DRS, and EDS technologies. Unexpectedly, light-reduced Ag^0 were generated owing to the reduction of AgI on the series of $\text{Ag}_2\text{O}/\text{AgI}$ composites with different content of Ag_2O , during the photocatalytic degradation of Rhodamine B (RhB) solution under visible light irradiation at room temperature, which can be confirmed by the results of XPS analysis. Thereby, there are the loaded noble metal nanoparticles (Ag NPs) in these systems which may cause localized surface plasmon resonance (SPR) effect [30–32]. The $\text{Ag}_2\text{O}/\text{AgI}$ with the assistant of plasmonic Ag NPs exhibits strong visible light absorption and superior photocatalytic activity compared with pure Ag_2O and AgI . The photocatalytic enhancement is supposed to stem from the strong SPR of Ag NPs on the surface of composites, which increase effective charge transfer and impede the recombination of the photogenerated electron-hole pairs during the photocatalytic reaction [33]. Finally, the probable mechanism of the composites was also proposed in detail.

2. Experimental section

2.1. Sample preparation

All chemicals were of analytical purity and applied without further purification. The $\text{Ag}_2\text{O}/\text{AgI}$ composites were prepared by a facile two-step precipitation method at room temperature. In a typical synthesis, 0.166 g of KI and 0.1699 g of AgNO_3 were dissolved in 20 mL deionized water under constant stirring at room temperature, respectively. Subsequently, the AgNO_3 solution was dropped into the KI solution with continuous stirring, respectively. After 30 min of stirring, the resulting yellow suspension was then filtered, washed several times with deionized water, and finally dried at 50 °C for 12 h.

The obtained products of AgI (0.2348 g) were dispersed into 20 mL distilled water under magnetic stirring for 30 min. Then, 0.1699 g of AgNO_3 dispersed into 10 mL of distilled water and the solution was added dropwise into the above suspension for 30 min of stirring. The 10 mL of NaOH (0.04 g) solution was subsequently added to the above mixture and stirred vigorously for 30 min. Finally, the final product was centrifuged, washed with deionized water, and dried at 50 °C for 12 h. For comparison, other $\text{Ag}_2\text{O}/\text{AgI}$ composites with theoretical molar ratios of Ag_2O to AgI (1:2, 1:1, 2:1) were also prepared under the same conditions. Meanwhile, pure AgI and Ag_2O particles were also prepared according to the same preparation procedure of $\text{Ag}_2\text{O}/\text{AgI}$ composites without addition of Ag_2O or AgI .

2.2. Characterization

The X-ray diffraction (XRD) studies for phase identification were performed using an X-ray diffractometer (Thermo ARL SCINTAG X'TRA) with $\text{CuK}\alpha$ radiation ($\lambda = 0.154,056$ nm), the operation voltage and current maintained at 40 kV and 40 mA and with the 2θ ranging from 10° to 80°. Scanning electron microscopy (SEM) images of the obtained products were taken with a Hitachi S-4700 field emission scanning electron microscope (SEM, scanning voltages 15 kV). EDS analysis were performed on an Energy-dispersive X-ray detector (EDS, Thermo Noran VANTAG-ESI). The X-ray

photoelectrons spectroscopy (XPS, ThermoESCALAB250, USA) was employed to examine the elemental compositions and chemical status of the samples. The UV–vis diffuse reflectance spectra (DRS) of the products were recorded on an UV–vis spectrophotometer (Lambda 850) equipped with an integrated sphere and using BaSO_4 as reference.

2.3. Photocatalytic experiments

The photocatalytic activity of the synthesized $\text{Ag}_2\text{O}/\text{AgI}$, pure AgI and Ag_2O samples was evaluated with degradation of Rhodamine B (RhB) solution under visible light irradiation. In each experiment, 0.1 g of the as-prepared photocatalyst was dispersed within 200 mL of RhB dye solution with a concentration of 10 mg/L in a 500 mL quartz beaker. Prior to irradiation, the suspension was placed in dark and stirred continuously without irradiation for 30 min to establish the adsorption–desorption equilibrium of the RhB dye on the surface of the photocatalyst. After that, the suspension was subjected to visible light irradiation and the source of visible light was a 300 W Xe lamp with 420 nm cut off filter. During irradiation, at intervals of every 5 min, about 3 mL of suspension was continually collected and centrifuged at 10,000 rpm to remove the photocatalyst particles. The concentration of solution was analyzed by measuring the maximum absorbance at its characteristic adsorption peak of 553 nm for RhB using a UV759S UV–Vis spectrophotometer.

3. Results and discussion

Crystalline phase structure of the as-prepared samples was investigated by X-ray power diffraction. Fig. 1 shows the XRD patterns of the AgI , the Ag_2O and the $\text{Ag}_2\text{O}/\text{AgI}$ heterojunction compositions with different molar ratios of Ag_2O . It can be seen that all the observed diffraction peaks [(100), (002), (101), (102), (110), (103), (112)] of the pure AgI can be indexed to a hexagonal β - AgI phase (JCPDS card no. 09-0374), while all the diffraction peaks of pure Ag_2O are indexed to (110), (111), (200), (220), (311) planes of cubic Ag_2O (JCPDS Card No. 76-1393). The XRD patterns of $\text{Ag}_2\text{O}/\text{AgI}$ heterojunction are comprised of two phases from AgI and Ag_2O , which indicates the coexistence of both AgI and Ag_2O phases. Moreover, no diffraction peaks assignable to Ag^0 (JCPDS no.65-2871) phase can be observed, indicating that the Ag_2O in the

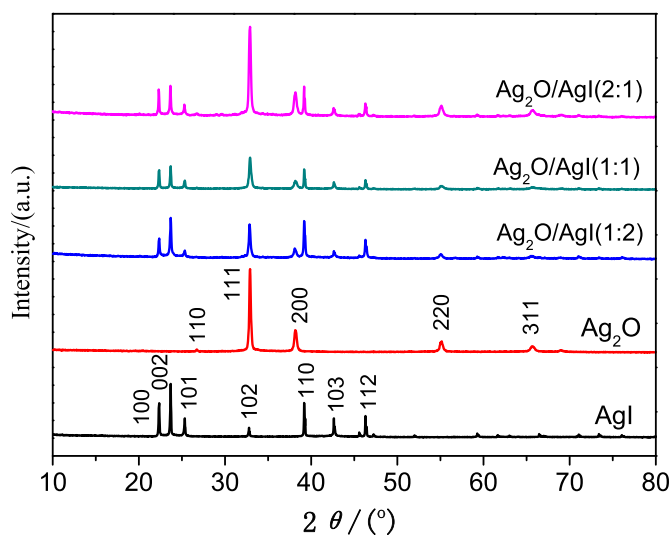


Fig. 1. XRD patterns of pure Ag_2O , AgI , and $\text{Ag}_2\text{O}/\text{AgI}$ with different molar ratios.

$\text{Ag}_2\text{O}/\text{AgI}$ composites has not decomposed during the synthesis process of as-prepared samples.

Fig. 2 presents the surface morphologies of the AgI, the Ag_2O and the $\text{Ag}_2\text{O}/\text{AgI}$ heterojunction with the molar ratio of 1:1. The SEM image of the pure AgI shown in Fig. 2a revealed that the obtained sample has a smooth surface and features an irregularly spherical-like microparticle structure with a diameter of 2–10 μm . In contrast, the images of Ag_2O in Fig. 2b has a spherical shape with smaller sizes of around 100–300 nm than those of AgI. For the $\text{Ag}_2\text{O}/\text{AgI}$ samples, as shown in Fig. 2c and d, some Ag_2O nanoparticles can be investigated nicely adhere to the AgI microparticles surface, indicating the formation of an intimate interfacial contact between the AgI and Ag_2O in the $\text{Ag}_2\text{O}/\text{AgI}$ composite. In addition, the element compositions of $\text{Ag}_2\text{O}/\text{AgI}$ were determined by EDS analysis (Fig. 2e). The peaks of Ag, I and O elements were detected in $\text{Ag}_2\text{O}/\text{AgI}$, which confirms the existence of $\text{Ag}_2\text{O}/\text{AgI}$. The molar

ratio of I:O existed in the $\text{Ag}_2\text{O}/\text{AgI}$ (mole ratio = 1:1) is calculated according to the EDS results to be 0.93: 1. STEM-EDS elemental mapping was also applied to obtain the elemental distributions in the $\text{Ag}_2\text{O}/\text{AgI}$ heterojunctions (Fig. 2f). It can be observed that Ag and I elements are homogeneously distributed in the AgI area, while O element from Ag_2O is distributed in the areas without AgI.

The surface elemental compositions and chemical status of the $\text{Ag}_2\text{O}/\text{AgI}$ (mole ratio = 1:1) composites were analyzed by XPS as shown in Fig. 3. Fig. 3a presents that the two strong peaks with a binding energy of 373.7 eV, 367.7 eV are attributed to Ag $3d_{3/2}$ and Ag $3d_{5/2}$ spectra of Ag^+ related to the Ag–O or Ag–I chemical bonding in $\text{Ag}_2\text{O}/\text{AgI}$, respectively. Fig. 3b shows that both of Ag $3d_{5/2}$ and $3d_{3/2}$ peaks can be deconvoluted into two separate peaks. The peaks at 373.6 eV and 367.7 eV can be assigned to Ag^+ ions, and those at 374.9 eV and 368.8 eV are ascribed to Ag^0 . This means the formation of Ag^0 during the RhB photodegradation process. Fig. 3c

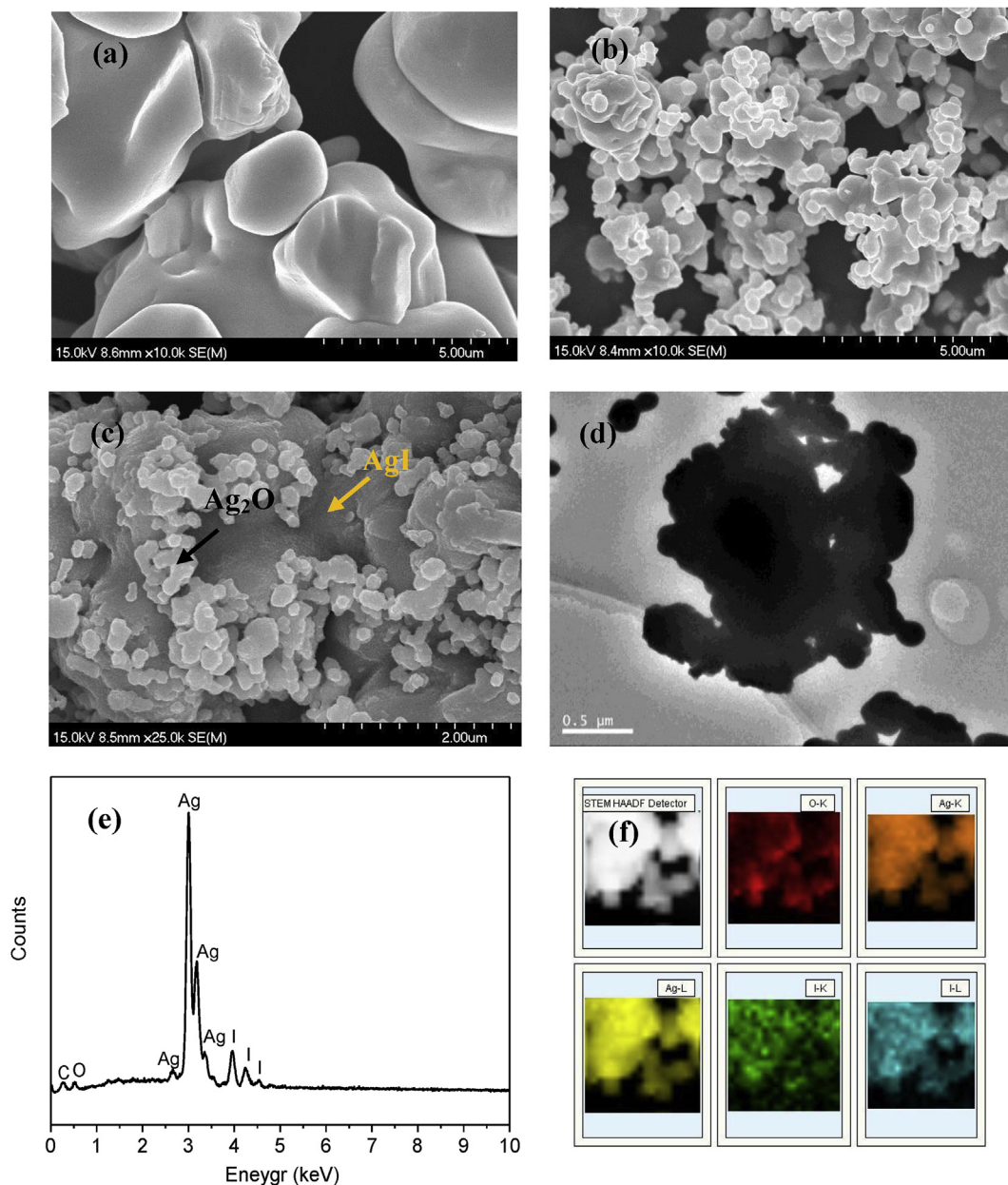


Fig. 2. SEM images of (a) AgI, (b) Ag_2O , (c) $\text{Ag}_2\text{O}/\text{AgI}$ (1:1), respectively. (d) TEM image, (e) EDS pattern, (f) STEM image of the $\text{Ag}_2\text{O}/\text{AgI}$ (1:1).

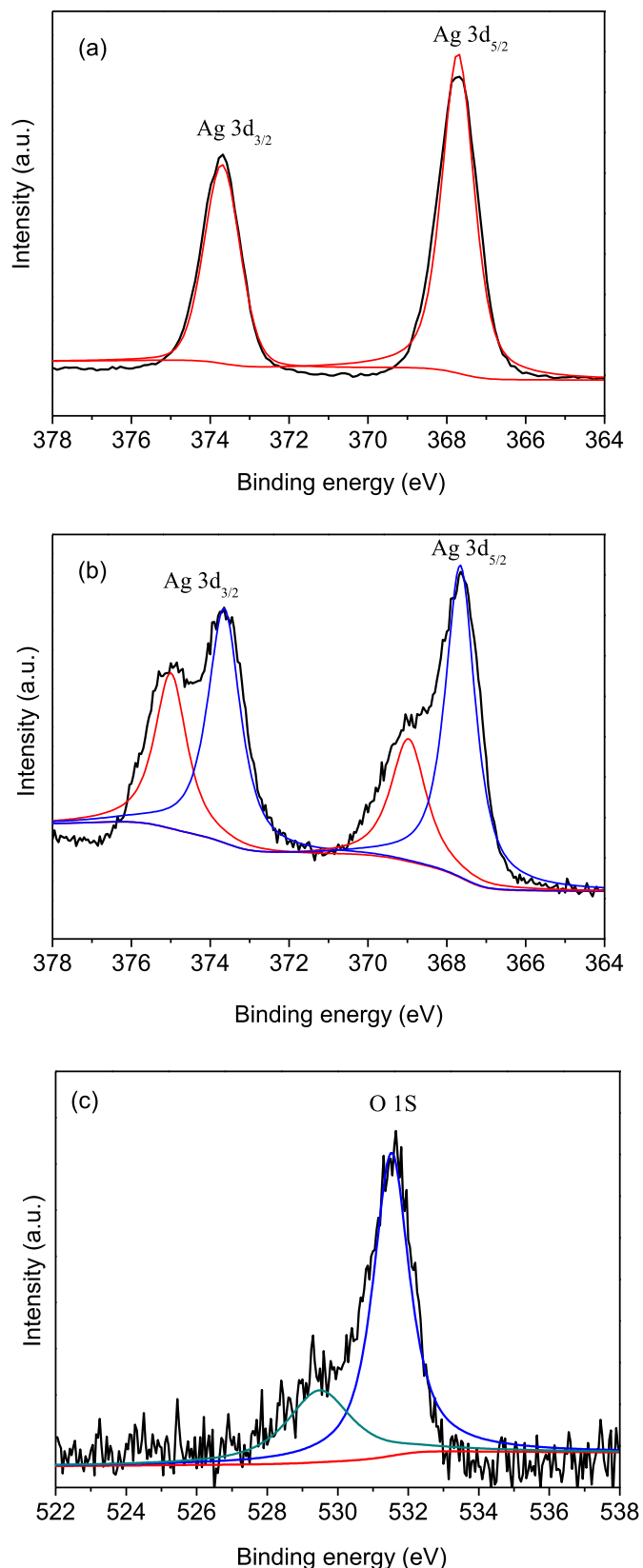


Fig. 3. High-resolution XPS spectra for the Ag 3d_{3/2} and Ag 3d_{5/2} of the fresh and used Ag₂O/AgI (1:1) (a) before photocatalysis and (b) after photocatalysis; (c) The High-resolution XPS spectra of O1s.

displays the XPS spectrum of the O 1s region of Ag₂O/AgI (mole ratio = 1:1), which can be seen the O 1s peak consisted of a

dominant peak at 531.2 eV and another higher energy peaks at approximately 530.7 eV. The two peaks can be indexed to Ag–O bonding and O–H in the hydroxyl groups.

To investigate the optical properties of the obtained samples, the UV–vis diffuse reflectance spectra are measured for AgI, Ag₂O and the Ag₂O/AgI heterojunctions with various mole ratios, as shown in Fig. 4. The results present that pure AgI has absorption edge around 450 nm in the visible light region. For Ag₂O/AgI heterojunctions, its absorption intensity is enhanced gradually and higher than that of AgI with increasing of the Ag₂O content, and the absorption edge of Ag₂O/AgI shows an obvious red shift compared with the absorption of pure AgI due to the spectral superposition of Ag₂O and AgI, which indicates the formation of the Ag₂O/AgI heterojunction composites is in favor of improving the utilization of visible light and enhancing their photocatalytic activity.

Photocatalytic performances of pure AgI, Ag₂O and Ag₂O/AgI heterojunctions with different molar ratios of Ag₂O and AgI are evaluated by measuring the degradation of RhB under the visible light irradiation, as shown in Fig. 5a. The results exhibit that the RhB decomposition rate for pure Ag₂O and AgI after 25min visible light irradiation can reach only 40% and 42%. However, there is a significant increase of photodegradation efficiency of RhB for Ag₂O/AgI heterojunctions composites, which is higher than those of the pure AgI and the Ag₂O. In addition, with increasing the molar ratio of Ag₂O to AgI, the photocatalytic activity of Ag₂O/AgI heterojunction has been promoted gradually with the degradation rate reaching 88% for Ag₂O/AgI (1:2) and a maximum rate of 99% for Ag₂O/AgI (1:1). However, the photocatalytic degradation rate decreases to 85% with the molar ratio is further increased owing to the excessive trapping sites resulted from excessive Ag₂O content in the Ag₂O/AgI composite, which may promote the recombination of photogenerated electron–hole pairs. With the mole ratio of 1:1, Ag₂O/AgI exhibits the highest photocatalytic activity, suggesting that the optimal mole ratio of Ag₂O and AgI is 1:1. The visible light absorption spectral changes of the degradation of RhB dye by the Ag₂O/AgI (1:1) catalyst was shown in Fig. 5b. It is observed that the absorbance peak at 552 nm becomes weak significantly in the presence of the Ag₂O/AgI heterostructure (1:1) as the irradiation time increases (Fig. 5b), which suggests that RhB was effectively photodegraded over the Ag₂O/AgI heterojunctions after 25 min. The total organic carbon was also measured which showed approximately 47.6% of removing after 25 min of reaction time. In

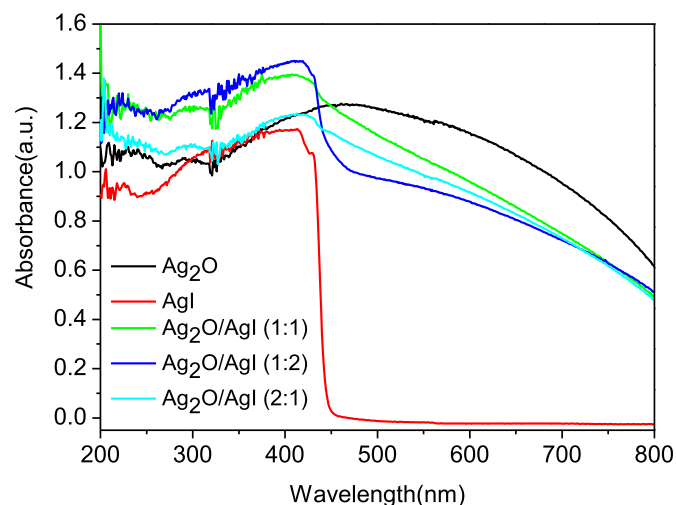


Fig. 4. UV–vis diffuses reflectance spectra of pure AgI, Ag₂O and Ag₂O/AgI composites (1:1, 1:2, 2:1).

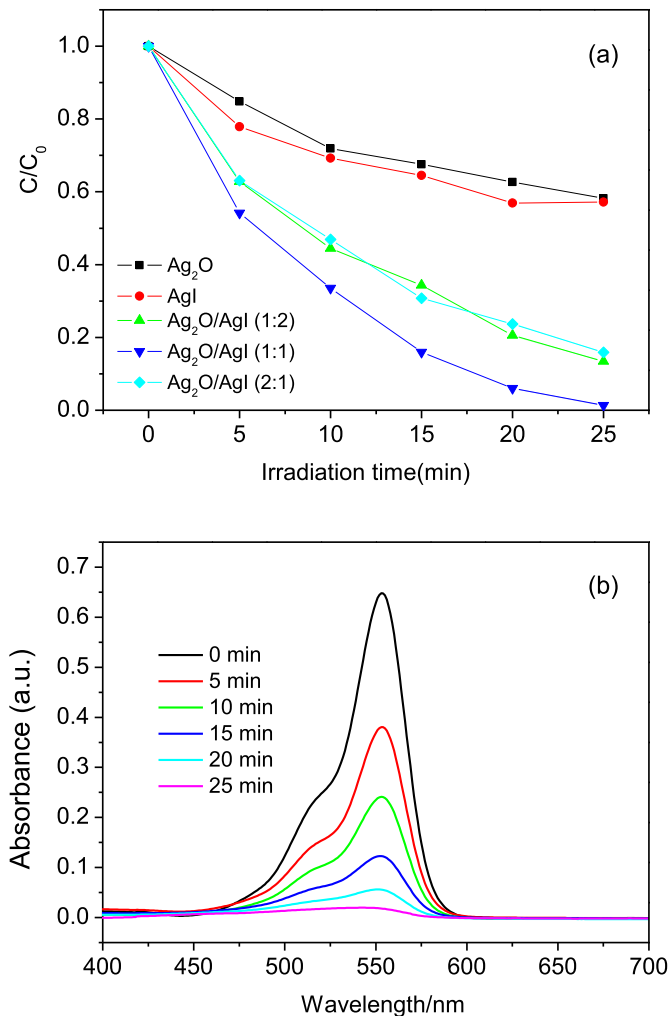


Fig. 5. (a) The photocatalytic activity of pure AgI, Ag₂O and Ag₂O/AgI composites with different Ag₂O contents, (b) visible light absorption spectral changes of the degradation of RhB dye by the Ag₂O/AgI (1:1) catalyst.

addition, the specific surface areas of those heterostructures were measured to investigate the influencing factors during the photocatalytic reaction. The result shows that the S_{BET} values of Ag₂O, Ag₂O/AgI (2:1), Ag₂O/AgI (1:1), Ag₂O/AgI (1:2) and AgI were 18.2, 15.5, 14.7, 12.3 and 8.1 m²/g, respectively. As can be seen the BET specific surface area increases with the increase of Ag₂O content. However, Ag₂O/AgI (1:1) other than Ag₂O showed the highest photocatalytic activity, indicating that the BET surface areas may not be the major factor in affecting the photocatalytic activity.

The RhB degradation process corresponding to pseudo-first-order reaction kinetics can be discussed with a Langmuir–Hinshelwood model (at low dye concentration):

$$\ln(C/C_0) = kt$$

Where k is the pseudo-first-order rate constant (min⁻¹) and t is the irradiation time. Moreover, C/C_0 is the ratio of the dye concentration at various intervals of irradiation time (min) and equilibrium concentration of the dyes after 30 min dark adsorption. As shown in Fig. 6b, the plots of $\ln(C/C_0)$ against the irradiation time (t) have a nearly linear relationship. The rate constants (k) of the AgI, Ag₂O and Ag₂O/AgI heterojunctions (mole ratio = 1:2, 1:1, 2:1) for the degradation kinetics of RhB are 0.024, 0.027, 0.079, 0.130,

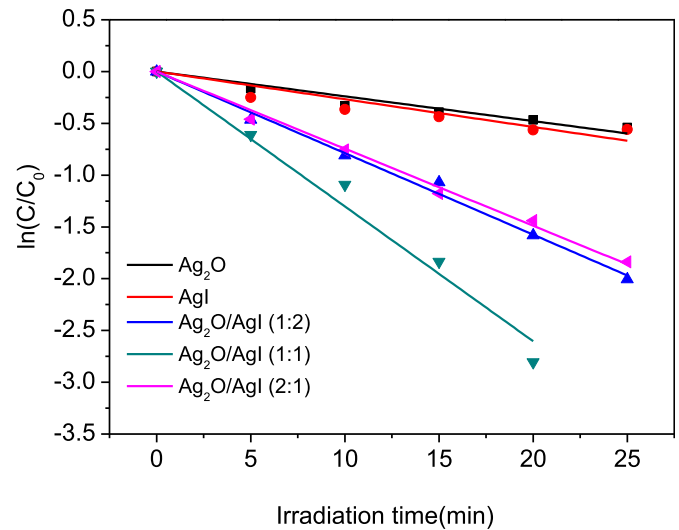


Fig. 6. The plot of $\ln(C/C_0)$ versus irradiation time curves of RhB degradation over AgI, Ag₂O and Ag₂O/AgI composites (1:1, 1:2, 2:1).

0.074 min⁻¹, respectively. Thus, Ag₂O/AgI (1:1) heterojunctions show the highest photocatalytic activity under visible light irradiation. To study the stability of the photocatalysts, Ag₂O/AgI (1:1) heterojunctions was tested in recycling reaction and the result is displayed in Fig. 7. It can be discovered that although there is deactivation of catalyst in every cycling runs, the photocatalytic activity of Ag₂O/AgI is still retained nearly 90% of its original photocatalytic activity in the third experimental run, suggesting that the heterojunctions catalyst possesses excellent stability.

To further investigate the photocatalysis mechanism of RhB degradation in detail, it's necessary to ascertain the main active species including hydroxyl radicals ($\cdot\text{OH}$), superoxide radical ($\cdot\text{O}_2^-$) and holes (h^+), which participate in the photocatalytic process. The radical scavengers of benzoquinone (BQ), isopropyl alcohol and ammonium oxalate are added to the RhB dye solution as the quenchers of $\cdot\text{O}_2^-$, $\cdot\text{OH}$ and h^+ , respectively. It can be observed that the presence of BQ and isopropyl alcohol significantly inhibited the degradation, which indicates the $\cdot\text{O}_2^-$ and $\cdot\text{OH}$ generated in the reaction process (see Fig. 8). However, when the ammonium oxalate is added to the system, the degradation rate of RhB has a slight

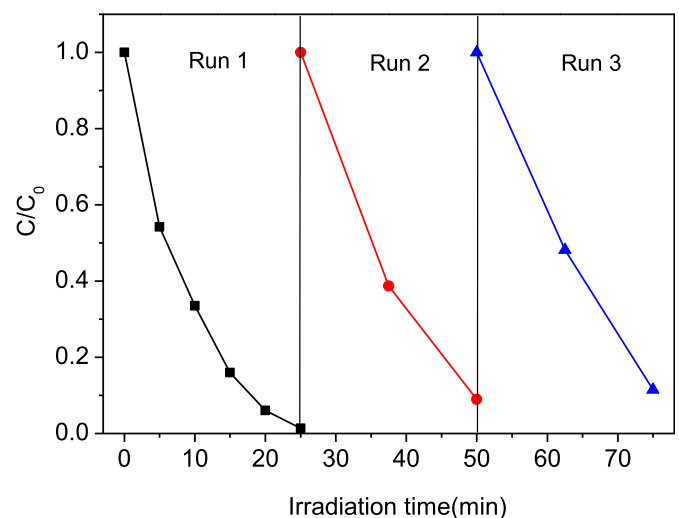


Fig. 7. The recycling efficiency of the Ag₂O/AgI composites (1:1).

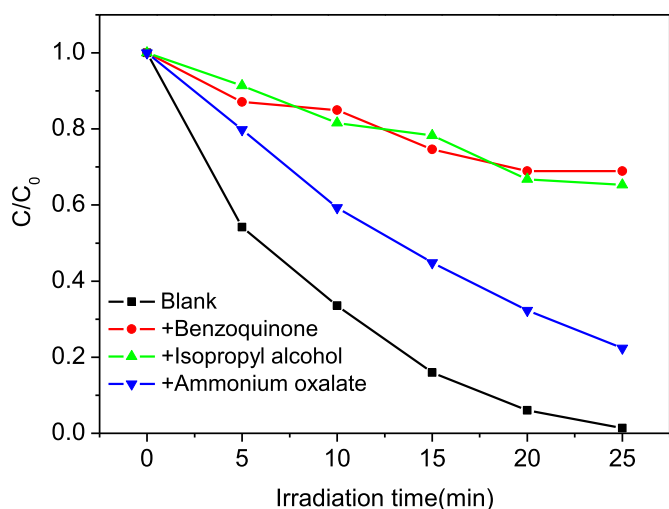
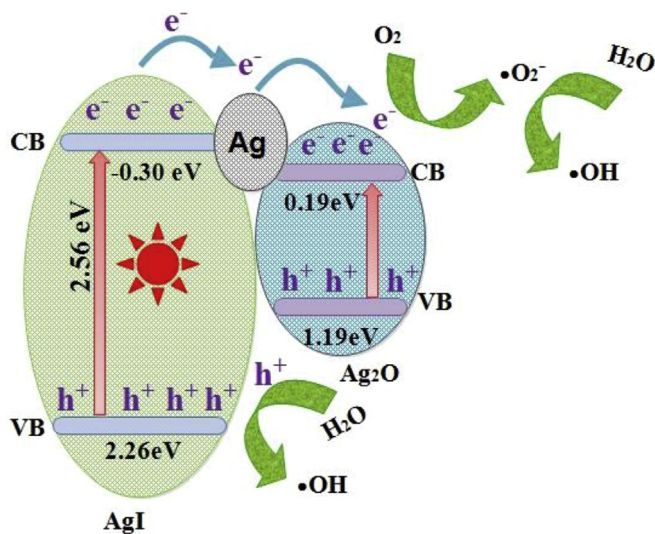


Fig. 8. Trapping experiment of active species during the photocatalytic degradation of RhB over $\text{Ag}_2\text{O}/\text{AgI}$ composites (1:1) under visible light irradiation.

decrease, implying that holes can be produced but not the main reactive species. Thus, the $\cdot\text{O}^{2-}$ and $\cdot\text{OH}$ as the reactive species play a crucial role on this photocatalytic process.

The possible mechanisms for degradation of RhB is proposed and shown in Scheme 1. According to the above XPS analysis, the presence of Ag^0 was confirmed which is owing to the partial reduction Ag^+ ions on the surface of $\text{Ag}_2\text{O}/\text{AgI}$ during the RhB photodegradation process. Therefore, under visible light irradiation, the photogenerated electron–hole pairs can be formed on the surface of the excited $\text{Ag}_2\text{O}/\text{AgI}$ and the Ag NPs. The electrons (e^-) on the conduction band (CB) of AgI will transfer to the Ag NPs. Sequentially, owing to the fact that the conduction band of AgI has a more negative potential than that of Ag_2O , the energetic electrons on the Ag NPs as the best conductive metals can migrate quickly to the CB of Ag_2O and ultimately can be trapped by the surface adsorbed O_2 in solution to form $\cdot\text{O}^{2-}$, and then the $\cdot\text{O}^{2-}$ radicals combined with H_2O molecules to produce active $\cdot\text{OH}$ radicals. At the same time, the photogenerated h^+ remained in the valence



Scheme 1. Photocatalytic mechanism scheme of $\text{Ag}_2\text{O}/\text{AgI}$ under visible light illumination (>420 nm).

band (VB) of AgI, Ag and Ag_2O react directly with H_2O to produce oxidative $\cdot\text{OH}$ radicals, which induces the subsequent degradation of the RhB dye. Thus, the heterostructured $\text{Ag}_2\text{O}/\text{AgI}$ composites have the excellent photocatalytic activity deriving from the assistant of plasmonic Ag NPs and the generating $\cdot\text{OH}$ and $\cdot\text{O}^{2-}$ radicals.

4. Conclusion

In summary, $\text{Ag}_2\text{O}/\text{AgI}$ heterojunction composites doped with different Ag_2O are successfully synthesized via a facile two-step precipitation process at room temperature. The results display that the Ag_2O nanoparticles are dispersed uniformly on the surface of AgI, which results in the formation of heterojunction. Moreover, Ag^0 NPs can be generated on $\text{Ag}_2\text{O}/\text{AgI}$ composites after irradiation by visible light, which was confirmed by XPS analysis. Thus, the $\text{Ag}_2\text{O}/\text{AgI}$ with the assistant of plasmonic Ag NPs is beneficial for interfacial charge transfer and has greatly enhanced photocatalytic activity in comparison with that of Ag_2O and AgI for photo-degradation of RhB under visible light irradiation. The mole ratio of the $\text{Ag}_2\text{O}/\text{AgI}$ composites plays a crucial role in the photocatalytic performance and the optimized molar ratio was 1:1. The present work provides a highly efficient $\text{Ag}_2\text{O}/\text{AgI}$ with plasmon-induced Ag NPs heterostructured photocatalyst, which is a promising photocatalyst for organic pollutants abatement.

Compliance with ethical standard

Conflict of interest the authors declare that they have no conflict of interest.

Acknowledgment

This work is financially supported by the National Nature Science Foundation of China (No. 21273034).

References

- [1] J.H. Yi, L.L. Huang, H.J. Wang, H. Yu, F. Peng, J. Hazard. Mater. 284 (2015) 207–214.
- [2] D.D. Yu, J. Bai, H.O. Liang, T.F. Ma, C.P. Li, J. Mol. Catal. A Chem. 420 (2016) 1–10.
- [3] H.F. Cheng, B.B. Huang, P. Wang, Z.Y. Wang, Z.Z. Lou, J.P. Wang, X.Y. Qin, X.Y. Zhang, Y. Dai, Chem. Commun. 47 (2011) 7054–7056.
- [4] Amy L. Linsebigler, G.Q. Lu, John T. Yates, Chem. Rev. 95 (1995) 735–758.
- [5] T.X. Wu, G.M. Liu, J.C. Zhao, J. Phys. Chem. B 102 (1998) 5845–5851.
- [6] J. Cao, Y.J. Zhao, H.L. Lin, B.Y. Xu, S.F. Chen, J. Solid State Chem. 206 (2013) 38–44.
- [7] J.D. Li, W. Fang, C.L. Yu, W.Q. Zhou, L.H. Zhu, Y. Xie, Appl. Surf. Sci. 358 (2015) 46–56.
- [8] X.F. Wang, R. Yu, K. Wang, G.Q. Yang, H.G. Yu, Chin. J. Catal. 36 (2015) 2211–2218.
- [9] X.Y. He, C.G. Hu, Y. Xi, K.Y. Zhang, H. Hua, Mater. Res. Bull. 50 (2014) 91–94.
- [10] Debabrata Sarkar, Chandan. K. Ghosh, S. Mukherjee, Kalyan K. Chattopadhyay, ACS Appl. Mater. Interfaces 5 (2013) 331–337.
- [11] C.M. Liu, J.W. Liu, G.Y. Zhang, J.B. Zhang, Q.S. Wu, Y.Y. Xu, Y.Q. Sun, RSC Adv. 5 (2015) 32333–32342.
- [12] T.T. Li, S.L. Luo, Ceram. Int. 41 (2015) 13135–13146.
- [13] X.J. Liu, J.Y. Liu, H.P. Chu, J.L. Li, W. Yu, G. Zhu, L.Y. Niu, Z. Sun, L.K. Pan, C.Q. Sun, Appl. Surf. Sci. 347 (2015) 269–274.
- [14] A. Kadam, R. Dhabbe, A. Gophane, T. Sathe, K. Garadkar, J. Photochem. Photobiol. B 154 (2016) 24–33.
- [15] Y. Du, D.D. Tang, G.K. Zhang, X.Y. Wu, Chin. J. Catal. 36 (2015) 2219–2228.
- [16] Y.H. Cao, Q.Y. Li, Y.Y. Xing, L.L. Zong, J.J. Yang, Appl. Surf. Sci. 341 (2015) 190–195.
- [17] L. Chen, H. Hua, Q. Yang, C.G. Hu, Appl. Surf. Sci. 327 (2015) 62–67.
- [18] M. Wu, J.M. Yan, X. W.Zhang, M. Zhao, Q. Jiang, J. Mater. Chem. A 3 (2015) 15710–15714.
- [19] D.D. Yu, J. Bai, H.O. Liang, T.F. Ma, C.P. Li, J. Mol. Catal. A Chem. 420 (2016) 1–10.
- [20] J. Yan, C. Wang, H. Xu, Y.G. Xu, X.J. She, J.J. Chen, Y.H. Song, Huaming Li, Qi Zhang, Appl. Surf. Sci. 287 (2013) 178–186.
- [21] N.K. Eswar, V.V. Katkar, P.C. Ramamurthy, G. Madras, Ind. Eng. Chem. Res. 54 (2015) 8031–8042.

- [22] P. Amornpitoksuk, S. Suwanboon, *Adv. Powder Technol.* 25 (2014) 1026–1030.
- [23] Y.Z. Li, H. Zhang, Z.M. Guo, J.J. Han, X.J. Zhao, Q.N. Zhao, S.J. Kim, *Langmuir* 24 (2008) 8351–8357.
- [24] R. Vinoth, P. Karthik, C. Muthamizhchelvan, B. Neppolian, M. Ashokkumar, *Phys. Chem. Chem. Phys.* 18 (2016) 5179–5191.
- [25] H.F. Ye, H.L. Lin, J. Cao, S.F. Chen, Y. Chen, *J. Mol. Catal. A Chem.* 397 (2015) 85–92.
- [26] D.J. Wang, L.L. Yue, L. Guo, F. Fu, X.M. Hea, H.D. Shen, *RSC Adv.* 5 (2015) 72830–72840.
- [27] H. Xu, Y.G. Xu, H.M. Li, J.X. Xia, J. Xiong, S. Yin, C.J. Huang, H.L. Wan, *Dalton Trans.* 41 (2012) 3387–3394.
- [28] H. Xu, J.X. Zhu, Y.X. Song, T.T. Zhu, W.K. Zhao, Y.H. Song, Z.L. Da, C.B. Liu, H.M. Li, *J. Alloys Compd.* 622 (2015) 347–357.
- [29] J. Chen, W.G. Mei, Q.J. Huang, N.N. Chen, C.L. Lu, H.J. Zhu, J. Chen, W.H. Hou, *J. Alloys Compd.* 688 (2016) 225–234.
- [30] D.D. Yu, J. Ba, H.O. Liang, J.Z. Wang, C.P. Li, *Appl. Sur. Sci.* 349 (2015) 241–250.
- [31] L. Jin, G.Q. Zhu, M. Hojamberdiev, X.C. Luo, C.W. Tan, J.H. Peng, Xi. M. Wei, J.P. Li, P. Liu, *Ind. Eng. Chem. Res.* 53 (2014) 13718–13727.
- [32] W. Xiong, Q. Zhao, X. Li, D. Zhang, *Catal. Commun.* 16 (2011) 229–233.
- [33] W.S. Wang, H. Du, R.X. Wang, T. Wen, A.W. Xu, *Nanoscale* 5 (2013) 3315–3321.